Leached Natural Saponite as the Silicate Source in the Synthesis of Aluminosilicate Hexagonal Mesoporous Materials

Thierry Linssen,*,† Pegie Cool,† Mohammed Baroudi,† Kristof Cassiers,† Etienne F. Vansant,† Oleg Lebedev,‡ and Joseph Van Landuyt‡

Laboratory of Adsorption and Catalysis, Department of Chemistry, University of Antwerp (UIA), Universiteitsplein 1, B-2610 Wilrijk, Belgium, and Centre for Electron Microscopy and Materials Science, University of Antwerp (RUCA), Groenenborgerlaan 171, B-2020 Antwerp, Belgium

Received: November 5, 2001; In Final Form: March 1, 2002

A new successful short time synthesis route for the preparation of FSM is developed using the leached natural aluminosilicate saponite, in combination with a low concentration of cetyltrimethylammoniumbromide [$C_{16}H_{33}N^+(CH_3)_3Br^-$ or CTMA] as surfactant. The leaching of the smectite increases with higher acid concentrations (5−10 M HCl) and temperature (25 °C and 100 °C). The leached saponite generated by these acid treatments allows the formation of mesoporous aluminosilicate hexagonal structures (FSM-16) with high porosity (max. 0.6 cm^3/g), high specific surface area (max. 900 m^2/g), thick pore wall, and uniform pore structure.

Introduction

Acid treatments of clay minerals modify their surfaces producing an increase in the specific surface area by disaggregation of clay particles, elimination of several mineral impurities, and dissolution of the external layers. At the same time, the number of acid centers of the treated solids also increases with respect to the parent clays. Thus, acid treatments have been used widely to increase the surface area of clay minerals and for obtaining from these minerals solids with a high porosity and high numbers of acid centers.[1−6] Acid activation consists, essentially, of treatment of the clay with acid solutions, the acids H_2SO_4, HNO_3 and, especially, HCl being used. The intensity of the treatment is determined by factors such as the nature and concentration of the acid used, treatment time, temperature, etc. During the treatments, variable amounts of the structural cations of the clay are removed, depending on the chemical composition and structure of the clay and on the intensity of the acid treatment.[4] If the treatment is aggressive enough, the octahedral cations are dissolved with the rates of depletion generally following the order $Mg^{2+} > Fe^{2+}$, $Fe^{3+} > Al^{3+}$ while the tetrahedral sheet forms amorphous silicate gel, insoluble in the acid solutions. These silicates are contaminated by small amounts of the remaining cations, especially the aluminum originally present in the tetrahedral sheets of the clays.[2]

The general mechanism for the depletion of metal ions from the octahedral sheet of 2:1 layered structures, studied by Kaviratna et al.,[2] involves proton attack at the edges of the layers. Evidence for edge attack is provided in part by the dependence of hydrolysis rates on the particle size of a nonswelling clay. The edge attack mechanism has also been recognized in the case of swelling smectite clays; however, hydrolysis occurring by proton attack through the ditrigonal cavities of the basal surfaces, known as gallery access mechanism, also has been evidenced.

Saponite is one of the most important trioctahedral smectites, originated as a product of the hydrothermal alteration and weathering of basalts and ultramafic rocks.[7] Saponite has a negatively charged tetrahedral sheet constituted of Si with impurities of Al^{3+}, partially balanced by the positive charge of the octahedral sheet constituted of Mg^{2+} with impurities of Fe^{2+} and Fe^{3+}.

The structural transformation from ordered silicates to amorphous silicate during the acid treatment is usually followed by X-ray diffraction, while the removal of cations is studied by chemical analysis. IR spectroscopy is usually used as a routine characterization technique, the spectra of the parent clay and of the solids obtained after acid activation being compared.

The preparation of crystalline mesoporous materials by using a new template concept (molecular assembly templating) has attracted increasing attention because of their possible use as catalysts, molecular sieves, and hosts for inclusion compounds, since they can be designed to have larger pore sizes than zeolites.[4−13] Until the 1990's no crystalline material was synthesized possessing mesopores. In 1990, Yanigasawa et al.[8] proposed a pillaring method consisting of interlayer cross-linking of a single-sheet silicate kanemite ($NaHSi_2O_5 \cdot 3H_2O$) in an ion exchange reaction with organic cations. By calcination the silicate−organic complexes were converted to mesoporous materials with uniform pore size distributions. This synthesis method was modified by Inagaki et al.[9] in 1993, producing mesoporous materials called "Folded Sheet Materials" (FSM) caused by its formation mechanism. They reported the formation of a long-ranged hexagonally ordered material by an electrostatic quaternary ammonium directed rearrangement (folding) of the kanemite.[14] The layered organic−inorganic composites are formed by intercalation of the layered silicate using cationic surfactants, designated as "Folded Sheet Mechanism". However, nowadays the mechanism is thought to be different. A hexagonal structure is created by condensation of silicate, which consists of derivatives of kanemite sheets, through the formation of a mosaic of hexagonal domains.[15−18] Approximately at the same time researchers at Mobil reported a family of mesoporous

* Corresponding author. E-mail: linssen@uia.ua.ac.be.
† Department of Chemistry, University of Antwerp (UIA).
‡ Centre for Electron Microscopy and Materials Science, University of Antwerp (RUCA).

10.1021/jp015578p CCC: $22.00
Published on Web 03/30/2002

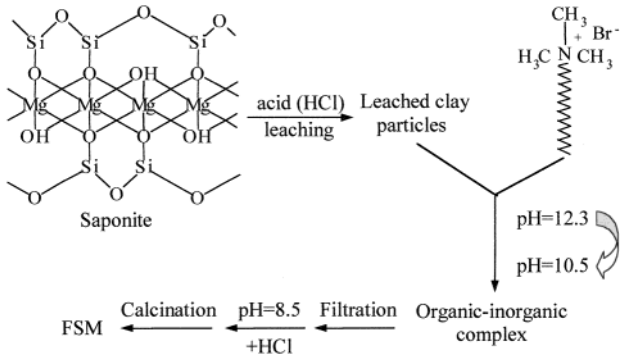

Figure 1. Procedure to synthesize FSM's starting from leached saponite.

materials (M41S) with a regular arrangement of mesopores[12] and proposed a "liquid-crystal template" (LCT) model for the formation mechanism.[13] MCM-41, one member of this family, exhibits the same structure as FSM having a hexagonal arrangement of uniform mesopores.

Interest in the silicon-based mesoporous materials, M41S, has expanded since it was shown that atoms other than silicon could be introduced in the wall. Further investigations have clearly illustrated catalytic applications for the mesoporous family especially for the MCM-41 structures.[19−22] Recently, the synthesis of mesoporous FSM aluminosilicates from layered silicates containing aluminum is also reported.[23−25]

In this paper we report on the optimization of the synthesis of FSM containing framework aluminum from leached natural saponite in order to synthesize mesoporous materials with acidic surface properties in a short synthesis time (3 days instead of 15 days for the FSM synthesized from kanemite) and low surfactant concentration (3 wt % instead of 26 wt % for the MCM-41 synthesis). These aluminosilicates are synthesized in different acidic media by varying the HCl concentration, resulting in mesoporous materials with optimized crystallinity, pore volume, and specific surface and variable aluminum concentrations rendering important potential as acid catalyst.

Experimental Section

(a) Materials. Saponite from near Ballarat (California), supplied by the Source Clay Repository of the Clay Minerals Society is used in this work. The clay contains up to 3% diopside and tremolite, separable by wet sedimentation. Saponite, a natural trioctahedrical clay with a TOT-structure has an octahedrical layer consisting of mainly $Mg(O, OH)_6$-octaheders condensed between two tetrahedrical layers consisting of mainly $Si(O, OH)_4$-tetraheders (see Figure 1). Sodium ions are located in the interlayer region to compensate for the negative charge on the sheets. The idealized chemical formula is $Na_{0.32}Ca_{0.38}(Si_{7.54}Al_{0.76})Mg_{5.22}O_{20}(OH)_4$. The exchangeable ions provide the untreated saponite a cation-exchange capacity (CEC) of 1.04 mmol/g. The size of the clay platelets used is $<2\mu$m in diameter and 0.96 nm in height.

(b) Sample Preparation. The natural saponite (2.5 g) was leached under stirring at 25 °C and at 100 °C for 24 h by, respectively, 20 mL of 6−10 M (Sap6/25, Sap7/25, Sap8/25, Sap9/25, and Sap10/25) and 3−7 M (Sap3/100, Sap4/100, Sap5/100, Sap6/100, and Sap7/100) HCl aqueous solutions to remove the magnesium-containing octahedral layer. The leached silicate powders were washed and filtered several times to remove all HCl.

The aluminosilicate FSM precursors were prepared according to Inagaki's method.[9,26] The leached saponites were suspended in 20 mL of solution using 0.1 M hexadecyltrimethylammonium bromide (HDTMABr) as structure directing agent and 1 g of the dried leached silicate powders (Sap6/25, Sap7/25, ..., Sap3/100, Sap4/100, ...) as silicate source, and denoted correspondingly as FSM(Sap6/25), FSM(Sap7/25), ..., FSM(Sap3/100), FSM(Sap4/100), ... The suspension was adjusted to a pH of 12.3 with 2 M NaOH and stirred for 3 h at 70 °C. After 3 h the solid was filtered and dispersed in 20 mL of distilled water and the pH of the dispersion was adjusted to 8.5 with 2 M HCl. This suspension was stirred for a subsequent 3 h at room temperature. All the samples were calcined at 550 °C for 6 h in air with a heating rate of 2 °C/min to obtain the mesoporous structure (Figure 1).

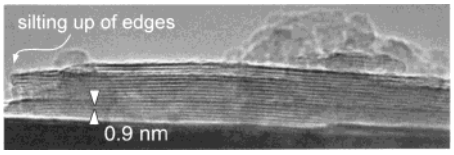

Figure 2. Magnified transmission electron micrograph of the acid-treated clay Sap8/25.

(c) Characterization Methods. The chemical compositions of the saponite and the leached saponites were determined by Atomic Absorption Spectrometry (AAS) using a UNICAM 969. The apparatus was equipped with an air−acetylene flame for Mg and an air−nitrous oxide flame for Al together with the conventional hollow cathode Mg and Al lamps. The conditions recommended by the manufacturer have been applied. The samples were first destructed in $HClO_4/HF/H_2BO_3$ under boiling conditions to remove the silicium. Next they were redissolved in HCl and diluted with a 0.5 M HNO_3 solution to analyze.

X-ray powder diffractograms (XRD) were measured on a Philips PW 1840 powder diffractometer with Cu K_α radiation (λ = 1.540 Å), 45 kV, 30 mA, and a Ni-filter. The samples were measured as powders.

Nitrogen adsorption−desorption isotherms of the calcined FSM materials were recorded at 77 K on a Quantachrome Autosorb-MP automated gas adsorption system. The samples are degassed at 150 °C during 16 h in a vacuum furnace prior to analysis. Surface areas are calculated according to the BET-equation, while the total pore volumes have been calculated from the adsorbed amount at a relative pressure $p/p_0 = 0.98$. Pore size distributions are obtained following the method of Barrett, Joyner and Halenda (BJH).

Diffuse reflectance infrared (DRIFT) spectra, following the different processes occurring during the acid activation of silicates, is recorded on a Nicolet 20 SXB FTIR spectrometer, equipped with a Spectra-Tech diffuse reflectance accessory. The resolution of the spectrum is 4 cm^{-1}.

TEM investigations were carried out with a JEOL 4000EX microscope operated at 400 kV to analyze the structure of the clay and leached clays. The point resolution of the microscope is of the order of 0.17 nm.

Results and Discussion

Upon acid activation of natural saponite the octahedral Mg^{2+} cations are removed. X-ray diffraction shows the partial destruction of the ordered structure of the clay. In the 2θ range between 25 and 30° a wide band of silicate gel is appearing while the narrow saponite bands are also retained. It is believed that the clay is partially dissolved forming amorphous silicate while a certain percentage of the saponite is preserved.

This hypothesis is also confirmed by a TEM picture taken after the acid leaching step (Figure 2) showing amorphous

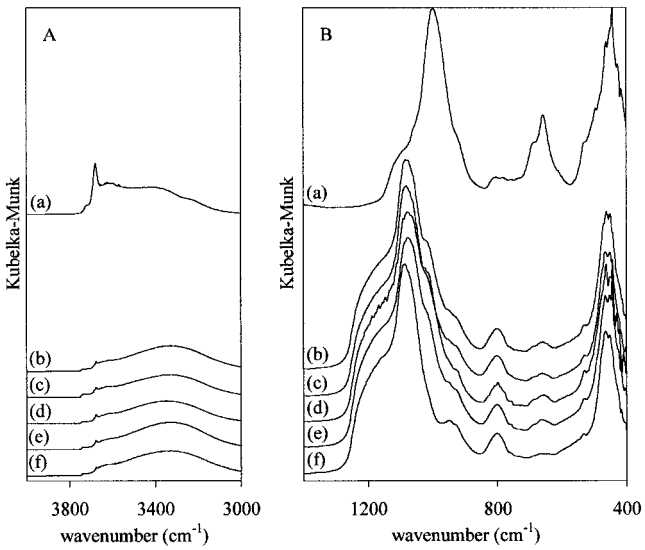

Figure 3. Diffuse reflectance infrared spectra in the 4000−3000 cm^{-1} region (A) and the 1400−400 cm^{-1} region (B), of untreated (a) and leached saponite: Sap6/25 (b), Sap7/25 (c), Sap8/25 (d), Sap9/25 (e), and Sap10/25 (f).

material and a layered structure with the thickness of the layers corresponding well with the postulated thickness (0.96 nm) of natural saponite. During the acid leaching of smectites the edge attack mechanism occurs abundantly in comparison with the gallery access mechanism.[2] The preservation of the clay under the acid treatment can be attributed to the formation of aggregates in such a way that a part of the clay is no more accessible for the acidic reagents. The TEM picture shows the silting up of the edges of the parallel ordered plates with amorphous material, partially preventing the edge attack mechanism during the leaching step. This amorphous material points out the partial dissolution of the clay during the leaching procedure.

The infrared (DRIFT) spectra of raw saponite and of the acid-treated samples are displayed in Figures 3A and 3B. In Figure 3A, the region between 4000 and 3000 cm^{-1} is shown and bands corresponding to water molecules and OH groups can be observed. In Figure 3B, characteristic bands due to the silicate structure appear between 1400 and 400 cm^{-1}. Some differences between the natural and the leached products can be observed.

As indicated, changes in the hydroxyl groups and in the water molecules bonded to the different metallic cations are observed in the spectra at high wavenumbers. The bands are due to different types of water molecules in the structure of the clay (adsorbed, coordinated, and zeolitic water), and to the presence of OH groups coordinated to the metallic cations, especially Mg−OH bonds. The band at 3675 cm^{-1}, assigned to the bending vibrational mode of Mg−OH, is decreasing in intensity during the acid leaching.[27] Also the band at 3635 cm^{-1}, corresponding to water bonded to the octahedral cation Mg^{2+}, decreases in intensity when these cations are removed by acid leaching. The wide band centered at about 3328 cm^{-1} and corresponding to the water adsorbed by the resulting amorphous silicate is only observed in this region in the activated solids pointing out the leaching of the saponite. The band at 1635 cm^{-1} (not shown here), due to the bending vibrational mode of water, remained, but decreased in intensity after the treatment. The removal of the octahedral cations is causing the loss of water and hydroxyl groups coordinated to them.

Between 1400 and 400 cm^{-1}, bands characteristic to silicate can be observed, mainly those corresponding to Si−O bonds in the tetrahedral sheet, and also to Mg−O stretching vibrational bonds. In saponite, the wide band centered at 997 cm^{-1}, characteristic of the tetrahedral sheet, is very sensitive to acid attack so its shape changes progressively, clearly showing the textural changes in the solids. During the treatment, this band shifts to higher wavenumbers while its shape changes characteristic for amorphous silicate gel in activated samples, appearing as a broad band centered at 1085 cm^{-1}. The shoulder at lower wavenumbers, indicates the tetrahedral sheet of saponite that has not been completely destroyed under the conditions employed for the acid activation. The tetrahedral sheet, with a characteristic band (shoulder) assigned to Si−O−Al bonds appearing at 527 cm^{-1}, is obviously more resistant to acid attack than the octahedral sheet, as evidenced by the disappearance of Mg−OH and Si−O−Mg band at, respectively, 664 cm^{-1} and 444 cm^{-1}. The solids obtained after activation are composed of both ordered saponite and amorphous silicate gel. In this sense, chemical analyses show that 42.3% of the Mg^{2+} cations (the main octahedral cation) are removed when it is treated with 8 M HCl at ambient temperature for 24 h (Sap8/25), while only 12.4% of the Al^{3+} cations (the main tetrahedral cation) are leached out. The formation of silicate is evidenced by the increase in intensity of the characteristic bands at 801 and 465 cm^{-1}.

A severe acid activation step is needed to leach out the Mg^{2+} cations in order to subsequently synthesize an optimal mesoporous FSM structure from the resulting amorphous silicate. The reason for this required high acid concentration is the silting up of the ends of the parallel ordered plates with amorphous material, partially preventing the edge attack mechanism during the leaching step.

During the acid leaching, variable amounts of the structural cations of the clay are removed, depending on the intensity of the acid treatment. In this paper the intensity of the treatment is determined by the acid concentration and the temperature. Above it has been proven that the applied treatment is aggressive enough to partially dissolve the octahedral Mg^{2+} cations while the tetrahedral sheet forms amorphous silicate gel, insoluble in the acid solutions. Subsequently these leached saponite clays were used as a silicate source in the synthesis of mesoporous aluminosilicate FSM materials in a short synthesis time. Searching for an optimal FSM the saponite is leached in different acidic media with varying HCl solutions and temperature in order to form mesoporous materials with maximal crystallinity, pore volume, and specific surface.

By analyzing the X-ray diffraction patterns and nitrogen adsorption isotherms at 77 K (Figures 4 and 5, respectively), the influence of the acid concentration during the leaching process on the crystallinity and structural properties of the synthesized mesoporous FSM's can be deduced. All samples exhibit at least one well-resolved reflection of an ordered hexagonal lattice in the low angle region between 2 and 10°. FSM materials with only one single peak exhibit a short-range hexagonal arrangement of pores as shown by Chen et al.[15] The shoulder of the basal peak is caused by diffuse higher order peaks. The presence of these peaks has been evidenced performing a deconvolution method on the XRD-patterns (deconvolution graphs not shown). The XRD results clearly show that the intensity of the d_{100} of the hexagonal unit cell of the FSM increases gradually with increasing acid concentration to reach a maximum at 8 M HCl and decreases with more severe treatments. The most condensed sample with the highest d_{100} (and *a*) value is the FSM(Sap8/25). Contrary to FSM materials

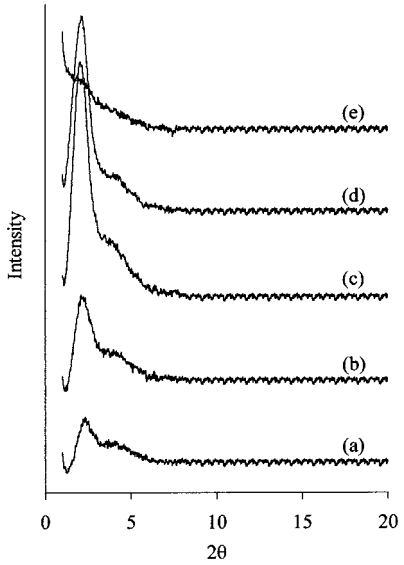

Figure 4. X-ray diffractograms of mesoporous FSM's synthesized from leached saponite at 25 °C: FSM(Sap6/25) (a), FSM(Sap7/25) (b), FSM(Sap8/25) (c), FSM(Sap9/25) (d), and FSM(Sap10/25) (e).

derived from kanemite the *d* spacing of FSM(Sap8/25) decreases upon calcination shown by a shift to higher 2θ.

The corresponding adsorption isotherm is of type IV in the BDDT classification and similar in shape to the nitrogen isotherm of a common FSM-16 from kanemite. Based on the nitrogen adsorption results, materials derived from leached saponite, e.g., sample FSM(Sap8/25) (see Table 1), show high surface area and fairly uniform pore size distribution (see Figure 5B). All the samples have a sharp step in their adsorption isotherms reflecting the filling of the mesopores (see Figure 5A). As derived from Horvath−Kawazoe analysis on adsorption isotherms, no micropores are present in these samples. Analyzing the corresponding nitrogen adsorption isotherm and its deduced pore size distributions (BJH-method) a pore size diameter of 3.0 nm was calculated for the optimal sample FSM(Sap8/25). Indeed also the nitrogen adsorption results clearly show that an optimum in BET surface area and nitrogen adsorption capacity is attained at FSM(Sap8/25), varying the intensity of the acid treatment.

Since for a hexagonal structure, the unit cell a_0 is the sum of the pore diameter and the thickness of the wall separating two adjacent pores, the value of the wall thickness can be calculated by subtracting the pore diameter (obtained by the BJH method) from the value of a_0. The results in Table 1 show a consistently larger wall thickness for the FSM structures in comparison with the MCM-41 materials. Combining the results from XRD and nitrogen adsorption, the wall thickness of these mesoporous materials is about 21 Å. The high pore wall thickness is a typical characteristic of FSM materials.[15−17]

The synthesized mesoporous structures are further studied by infrared spectroscopy (DRIFT). The infrared spectra of saponite (Figure 6a), treated saponite (Sap8/25) (Figure 6b), and the resulting mesoporous structure after synthesis (FSM(Sap8/25)) (Figure 6c) are shown in Figure 6A and 6B. The spectrum of amorphous silicate (Figure 6d) is also shown for reasons of comparison. In Figure 6A, the region between 4000 and 3000 cm^{-1} is shown and bands corresponding to water molecules and OH groups can be observed. In Figure 6B, characteristic bands due to the silicate structure appear between 1400 and 400 cm^{-1}.

The spectra at high wavenumbers have bands due to Mg−OH bonds and different types of water molecules in the structure

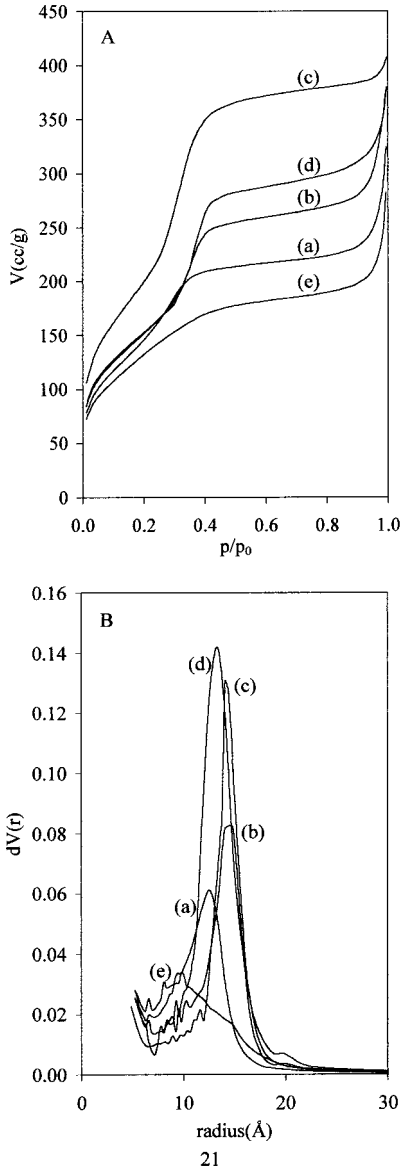

Figure 5. (A) N_2-adsorption isotherms at 77 K of mesoporous FSM's synthesized from leached saponite at 25 °C: FSM(Sap6/25) (a), FSM(Sap7/25) (b), FSM(Sap8/25) (c), FSM(Sap9/25) (d), and FSM(Sap10/25) (e). (B) The corresponding pore size distributions calculated following the BJH-method.

TABLE 1: BET Surface Areas, Pore Volumes, Tentative Pore Sizes, Unit Cell Dimensions and Subsequent Wall Thickness of Mesoporous FSM's Synthesized from Leached Saponite at 25 °C

sample	S_{BET} (m^2/g)[a]	PV (cc/g)[b]	Ø (nm)[c]	*a* (nm)[d]	*t* (nm)[e]
FSM(Sap6/25)	643	0.44	2.5	4.4	1.9
FSM(Sap7/25)	726	0.54	2.9	4.9	2.0
FSM(Sap8/25)	900	0.61	3.0	5.1	2.1
FSM(Sap9/25)	785	0.54	2.7	4.8	2.1
FSM(Sap10/25)	478	0.37	2.0		

[a] S_{BET} = Specific surface calculated with the BET method. [b] PV = Pore volume measured at a p/p_0 value of 0.98. [c] Ø = Mean diameter of the pore size distribution calculated with the BJH method. [d] *a* = Unit cell parameter calculated from the 100 reflection of the hexagonal structure. [e] *t* = Pore wall thickness calculated from the difference between a and Ø.

of the clay. The band of the bending vibrational mode of Mg−OH at 3675 cm^{-1} almost totally disappeared in the spectrum of the synthesized FSM structure. Apparently the synthesis conditions (initial pH of 12.3) bring about a further dissolution of

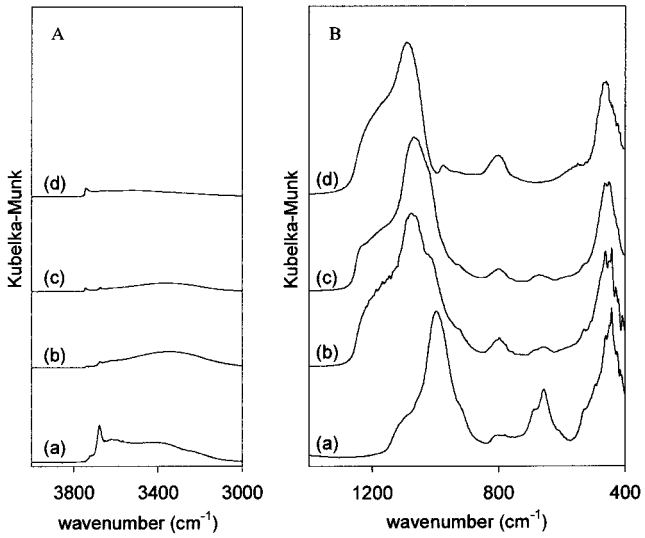

Figure 6. Diffuse reflectance infrared spectra in the 4000−3000 cm^{-1} region (A) and the 1400−400 cm^{-1} region (B), of untreated (a) and leached saponite: Sap8/25 (b), the resulting FSM(Sap8/25) (c), and amorphous silicate (d).

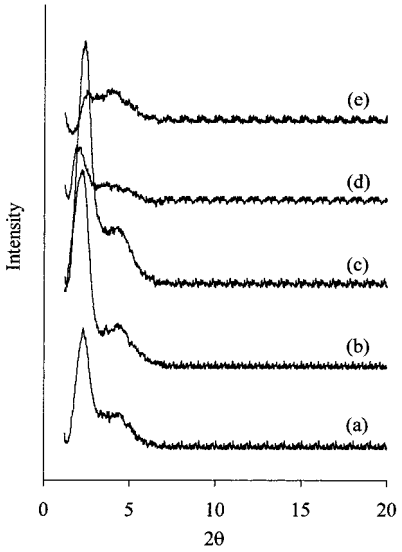

Figure 7. X-ray diffractograms of mesoporous FSM's synthesized from leached saponite at 100 °C: FSM(Sap3/100) (a), FSM(Sap4/100) (b), FSM(Sap5/100) (c), FSM(Sap6/100) (d), and FSM(Sap7/100) (e).

the octahedral Mg(II) cations. During the synthesis a band at 3740 cm^{-1} is appearing, pointing out the formation of isolated silanol groups in the final mesoporous material.

To study the textural changes of the solids the spectra between 1400 and 400 cm^{-1} are examined. The condensation of the FSM structure can be investigated with infrared spectroscopy (DRIFT) looking at the asymmetric absorption band at 1240 cm^{-1} of strained siloxane bridges. These siloxane bridges are situated at the surface of the pore walls, being more uniform in the case of a higher ordering of the mesopores and consequently crystallinity of the structure. Therefore, the intensity (or sharpness) of this band gives some information about the condensation degree and crystallinity of the synthesized materials.[28] Apparently the 1240 cm^{-1} band becomes more intense after calcination of the FSM(Sap8/25) material, pointing out a higher condensation degree (Figure 6c). Comparing this infrared spectrum with literature results of spectra from FSM synthesized from kanemite, a comparable crystallization degree can be deduced. The wide band centered at 997 cm^{-1} is characteristic of the tetrahedral sheet in saponite. Changing its shape progressively, it clearly shows the textural changes in the solids. During the different synthesis steps, this band shifts to higher wavenumbers and eventually takes a form characteristic for semicrystalline mesoporous materials (Figure 6c). This broad band centered at 1069 cm^{-1} is a superposition of different silicate infrared absorption bands, of which the major contribution is the asymmetric silicate stretching vibration. It has a shoulder at lower wavenumbers, indicating that the tetrahedral sheet of saponite has not been completely destroyed under the conditions employed during the synthesis. The Mg−OH and Si−O−Mg bands at, respectively, 664 cm^{-1} and 444 cm^{-1} disappeared in the FSM spectrum of the calcined mesoporous material (Figure 6c), indicating again the almost complete removal of the octahedral Mg(II).

The intensity of the treatment is determined not only by the acid concentration but also by the temperature. To study the effect of the temperature on the optimum in the leaching of the saponite and the resulting structure of the mesoporous FSM materials the same syntheses were carried out at 100 °C and characterized using the same techniques. It can be seen from Figures 7 and 8 that, when a higher temperature is applied during the leaching step, the optimal mesoporous structure results now

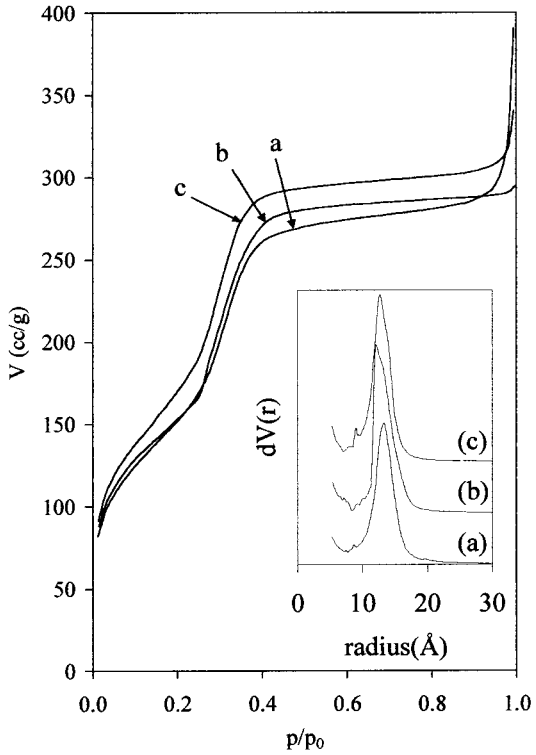

Figure 8. N_2-adsorption isotherms at 77 K of mesoporous FSM's synthesized from leached saponite at 100 °C: FSM(Sap3/100) (a), FSM(Sap4/100) (b), FSM(Sap5/100) (c). Inset: The corresponding pore size distributions calculated following the BJH-method.

from a saponite activation with lower acid concentration. The mesoporous FSM structure with the most intense hexagonal X-ray diffraction pattern is obtained after a treatment of the clay at 100 °C with a 4 M HCl solution for 24 h. Again, all the diffractograms apparently have only one single peak, with a shoulder caused by diffuse higher order peaks, in the low angle region because all samples have a short-range hexagonal arrangement of pores. The most condensed sample with the highest d_{100} (and a) value is the FSM(Sap5/100).

The corresponding nitrogen adsorption isotherms and the deduced structure characteristics indeed point out that the FSM(Sap5/100) is the optimal sample synthesized after a

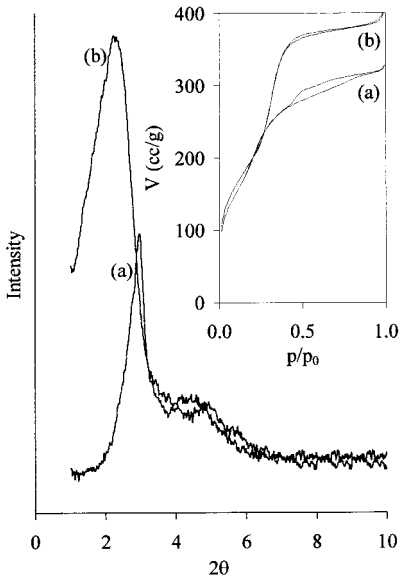

Figure 9. X-ray diffractograms of mesoporous FSM(Sap8/25) synthesized without (a) and with (b) filtration step. Inset: The corresponding N_2-adsorption isotherms at 77K.

TABLE 2: BET Surface Areas, Pore Volumes, Tentative Pore Sizes, Unit Cell Dimensions, and Subsequent Wall Thickness of Mesoporous FSM's Synthesized from Leached Saponite at 100 °C

sample	S_{BET} (m^2/g)	PV (cc/g)	Ø (nm)	*a* (nm)	*t* (nm)
FSM(Sap3/100)	521	0.50	2.7	4.5	1.8
FSM(Sap4/100)	539	0.45	2.4	4.7	2.3
FSM(Sap5/100)	575	0.98	2.5	4.3	1.8
FSM(Sap6/100)				5.3	
FSM(Sap7/100)				4.1	

leaching step at 100 °C. The attained BET surface area and nitrogen adsorption capacity, shown in Table 2, are however lower than those of FSM(Sap8/25). The FSM's synthesized after an acid leaching step at 100 °C again have a consistently larger wall thickness in comparison with MCM-41 materials.

During the synthesis a part of the leached clay is dissolved at pH = 12.3 and subsequently condensed at pH = 8.5 to amorphous silicate, as proven by the broad band in the XRD pattern at 2θ equal to ~25. When a filtration step was added to the synthesis of the mesoporous FSM after the 3 h of stirring at the initial pH, all the dissolved silicate should be removed, preventing the formation of amorphous silicate. The effect of this additional step on the structural properties of the mesoporous material is pictured in Figure 9 considering the XRD pattern and the N_2 adsorption−desorption isotherm of the FSM(Sap8/25) synthesized with (FSMf) and without (FSMnf) filtration step. In the X-ray diffractogram indeed the broad band has disappeared after the subsequent 3 h of stirring at a pH of 8.5. A significant improvement in the crystallinity can be observed by addition of the filtration step to the synthesis. Also, the substantial enhancement of the hexagonal cell parameter from $a = 4.4$ nm to 5.1 nm is of great interest. Moreover the nitrogen isotherms measured at 77 K of both samples show a similar pore size enlargement from $d = 2.2$ nm to 3.0 nm, while the pore size distribution becomes very narrow indicating a homogeneous distribution of hexagonal mesopores. In addition, the enhancement in pore volume (from 0.49 cm^3/g to 0.61 cm^3/g) and specific surface area (from 660 m^2/g to 900 m^2/g) for the materials synthesized with the filtration step suggests a general improvement of the mesoporous FSM structure. Therefore, for all the former syntheses reported in this paper the additional filtration step has been performed.

Conclusions

By this work it is proven that the leaching procedure of saponite results in a depopulation of octahedral cations and a progressive and partial destruction of the silicate ordered structure with the consequent formation of amorphous silicate gel. Subsequently these leached saponite clays were introduced as silicate source in the synthesis of mesoporous aluminosilicate hexagonal FSM structures (M41S family) in a short synthesis time and with a low concentration of surfactant. The mesoporous material with the most condensed structure, the highest unit cell dimension (5.1 nm), surface area (900 m^2/g), pore volume (0.61 cm^3/g) and a fairly narrow pore size distribution (3.0 nm) is the one synthesized after an acid leaching step with 8 M HCl at ambient temperature. Beside the acid concentration, also the temperature determines the intensity of the acid treatment, creating leached clay particles to synthesize an optimal mesoporous structure. Increasing the temperature from 25 °C to 100 °C during the leaching step brings about a lower acid concentration to synthesize an optimal FSM structure.

When a filtration step is added to the synthesis of the mesoporous FSM after the 3 h of stirring at the initial pH, all the dissolved silicate is removed preventing the formation of amorphous silicate. The additional step results in a general improvement of the mesoporous FSM structure giving rise to a significant higher crystallinity and a substantial enhancement of the hexagonal cell parameter from $a = 4.4$ nm to 5.1 nm.

Acknowledgment. T. Linssen is indebted to the IWT for financial support. P. Cool acknowledges the FWO Vlaanderen (Fund for Scientific Research-Flanders-Belgium) for financial support. O. Lebedev performed this work within the framework of IUAP 4/10.

References and Notes

(1) Vicente-Rodríguez, M. A.; Suárez, M.; Bañares-Muñoz, M .A.; López-González, J. de D. *Spectrochim. Acta A* **1996**, *52*, 1685.
(2) Kaviratna, H.; Pinnavaia, T. J. *Clay. Clay Miner*. **1994**, *42*, 717.
(3) Prieto, O.; Vicente-Rodríguez, M. A.; Bañares-Muñoz, M. A. *J. Porous Mater*. **1999**, *6*, 335.
(4) Komadel, P.; Madejova, J.; Janek, M.; Gates, W. P.; Kirkpatrick, R. J.; Stucki, J. W. *Clays Clay Miner*. **1996**, *44*, 228.
(5) Vicente-Rodríguez, M. A.; López-González, J. de D.; Bañares-Muñoz, M. A. *Microporous Mater*. **1995**, *4*, 251.
(6) Vicente-Rodríguez, M. A.; Suárez, M.; López-González, J. de D.; Bañares-Muñoz, M. A. *Langmuir* **1996**, *12*, 566.
(7) Post, J. L. *Clays Clay Miner*. **1984**, *32*, 147.
(8) Yanagisawa, T. *Bull. Chem. Soc. Jpn.* **1990**, *63*, 988.
(9) Inagaki, S.; Fukushima, Y.; Kuroda, K. *Chem. Soc., Chem. Commun*. **1993**, *8*, 680.
(10) Selvam, P.; Bhatia, S. K.; Sonwane, C. G. *Ind. Eng. Chem. Res.* **2001**, *40*, 3237.
(11) Ciesla, U.; Schüth, F. *Microporous Mesoporous Mater.* **1999**, *27*, 131.
(12) Kresge, C. T.; Leonowicz, M. E.; Roth, W. L.; Vartuli, J. C.; Beck, J. S. *Nature* **1992**, *359*, 710.
(13) Beck, J. S.; Vartuli, J. C.; Roth, W. J.; Leonowicz, M. E.; Kresge, C. T.; Smitt, K. D.; Chu, C. T.-W.; Olson, D. H.; Sheppard, E. W.; McCullen, S. B.; Higgins, J. B.; Schlenker, J. L. *J. Am. Chem. Soc*. **1992**, *114*, 834.
(14) Beneke, K.; Lagaly, G. *Am. Mineral*. **1977**, *62*, 763.
(15) Chen, C.-Y.; Xiao, S.-Q.; Davis, M.E. *Microporous Mater*. **1995**, *4*, 1.
(16) O'Brien, S.; Francis, R. J.; Price, S. J.; O'Hare, D.; Clark, S. M.; Okazaki, N.; Kuroda, K. *J. Chem. Soc., Chem. Commun*. **1995**, 2423.
(17) O'Brien, S.; Francis, R. J.; Fogg, A.; O'Hare, D.; Okazaki, N.; Kuroda, K. *Chem. Mater*. **1999**, *11*, 1822.
(18) Sakamoto, Y.; Inagaki, S.; Ohsuna, T.; Ohnishi, N.; Fukushima, Y.; Nozue, Y.; Terasaki, O. *Microporous Mesoporous Mater*. **1998**, *21*, 589.

(19) Corma, A.; Fornés, V.; Navarro, M. T.; Pérez-Pariente, J. *J. Catal.* **1994**, *148*, 569.
(20) Di Renzo, F.; Coustel, N.; Mendibourne, M.; Cambon, H.; Fajula, F. *Stud. Surf. Sci. Catal.* **1997**, *105*, 69.
(21) Zhao, D.; Nie, C.; Zhou, Y.; Xia, S.; Huang, L.; Li, Q. *Catal. Today* **2001**, *68*, 11.
(22) Eimer, G. A.; Pierella, L. B.; Anunziata, O. A. In *Zeolites and Mesoporous Materials at the Dawn of the 21st Century, Studies in Surface Science and Catalysis*; Galarneau, A., Di Renzo, F., Fajula, F., Vedrine, J., Eds.; Elsevier: Amsterdam, 2001; Vol. 135, p 199.
(23) Inagaki, S.; Yamada, Y.; Fukushima, Y. *Stud.n Surf. Sci. Catal.* **1997**, *105*, 109.
(24) Kan, Q.; Fornés, V.; Rey, F.; Corma, A. *Mater. Chem.* **2000**, *10*, 993.
(25) Linssen, T.; Barroudi, M.; Cool, P.; Vansant, E. F. In *Zeolites and Mesoporous Materials at the Dawn of the 21st Century, Studies in Surface Science and Catalysis*; Galarneau, A., Di Renzo, F., Fajula, F., Vedrine, J., Eds.; Elsevier: Amsterdam, 2001; Vol. 135, p 201.
(26) Inagaki, S.; Ogata, S.; Goto, Y.; Fukushima Y. *Stud. Surf. Sci. Catal.* **1998,** *117*, 65.
(27) Komadel, P.; Madejova, J.; Janek, M.; Gates, W. P.; Kirkpatrick, R. J.; Stucki, J. W. *Clays Clay Minerals* **1996**, *44*, 228.
(28) Collart, O.; Van Der Voort, P.; Vansant, E. F.; Desplantier, D.; Galarneau, A.; Di Renzo, F.; Fajula, F. *J. Phys. Chem. B*, in press.